QUANTUM CRITICALITY

Quantum critical points and the sign problem

R. Mondaini[1], S. Tarat[1], R. T. Scalettar[2]

The "sign problem" (SP) is a fundamental limitation to simulations of strongly correlated matter. It is often argued that the SP is not intrinsic to the physics of particular Hamiltonians because its behavior can be influenced by the choice of algorithm. By contrast, we show that the SP in determinant quantum Monte Carlo (QMC) is quantitatively linked to quantum critical behavior. We demonstrate this through simulations of several models with critical properties that are relatively well understood. We propose a reinterpretation of the low average sign for the Hubbard model on the square lattice away from half filling in terms of the onset of pseudogap behavior and exotic superconductivity. Our study charts a path for exploiting the average sign in QMC simulations to understand quantum critical behavior.

Over the past several decades, quantum Monte Carlo (QMC) simulations have provided great insight into challenging strong correlation problems in chemistry (*1*, *2*), condensed-matter physics (*3*, *4*), nuclear physics (*5*), and high-energy physics (*6*). In all of these areas, however, the sign problem (SP), which occurs when the probability for specific quantum configurations in the importance sampling becomes negative, substantially constrains their application. Solving, or at least mitigating, the SP is one of the central endeavors of computational physics. The extent and importance of the effort is indicated by the many proposed solutions and their continued development over the past three decades [for an overview, see the supplementary materials (*7*) and references therein].

Despite enormous effort, the SP remains unsolved. In fact, the lack of progress is one of the main driving forces behind a number of large-scale research efforts, including the quest for quantum emulators (*8*–*10*) and quantum computing itself (*11*, *12*). One of the most fundamental mysteries concerns the possible link between the SP and the underlying physics of the Hamiltonian being investigated.

Here, instead of challenging this nondeterministic polynomial hard problem (*13*) or proposing solutions that can partially ameliorate its behavior (*14*, *15*), we show that there is a clear connection between the behavior of the average sign $\langle S \rangle$ in the widely used determinant quantum Monte Carlo (DQMC) method and several quantum phase transitions (QPTs): that of the semimetal to antiferromagnetic Mott insulator (MI) of Dirac fermions in the spinful [SU(2)] honeycomb-Hubbard Hamiltonian (*16*, *17*), the band to correlated insulator transition (*18*–*20*), and charge density wave (CDW) transitions of spinless [U(1)] fermions on a honeycomb lattice (*21*, *22*). In the first example, simulations at half-filling, where the quantum critical point (QCP) occurs, are SP-free. We introduce a small doping μ and show, in the limit $\mu \to 0^+$ at temperature $T \to 0$, that $\langle S \rangle$ evolves rapidly as we tune through the QCP.

Our second illustration, the ionic Hubbard model, has an SP even at half-filling. Here, the average sign undergoes an abrupt drop at the band insulator (BI) to correlated metal (CM) transition. The third example, spinless fermions on a honeycomb lattice, also features a semimetal to (charge) insulator transition but allows for an SP-free approach. Studying it with a method that contains an "unnecessary" SP lends insight into the key question of the influence of different algorithms on the connection between the SP and the physics of model Hamiltonians.

These three discussions establish a link between known physics of the models and the fermion sign. Having made that connection, we turn to the iconic square lattice Hubbard model, the physics of which has not been conclusively established. We find that the onset of the SP occurs in a dome-shaped region of the filling-temperature phase space under that of the pseudogap physics. The SP is sufficiently well controlled in the pseudogap phase to obtain reliable results for various observables, including the pairing correlations in various channels, exhibiting dominant enhancement for *d*-wave symmetry. Because it behaves exponentially in inverse temperature, the SP provides a rather sharp demarcation of the regime, mimicking the superconducting dome of the cuprates (*23*). Although the SP prevents DQMC from resolving a signal of a *d*-wave transition, the groundwork established for the honeycomb lattice and BI-CM models suggests that this SP dome might be linked to the onset of a superconducting phase.

The SP: Model and methodology

The origin of the SP can be understood in two related classes of algorithms, world-line QMC (WLQMC) (*24*) and Green's function QMC (GFQMC) (*25*, *26*), by considering Feynman's path integral approach, which provides a mapping of quantum statistical mechanics in D dimensions to classical statistical mechanics in $D + 1$ dimensions. Paralleling Feynman's original exposition for the real-time evolution operator $e^{-i\hat{H}t/\hbar}$, the imaginary time evolution operator $e^{-\beta\hat{H}}$ is subdivided into L_τ incremental pieces $\hat{U}_{\Delta\tau} = e^{-\Delta\tau\hat{H}}$, where $\hbar$ is the reduced Planck's constant, $\hat{H}$ is the Hamiltonian, and $L_\tau\Delta\tau = \beta$ is the inverse temperature. Complete sets of states $I_\tau = \Sigma_{S_\tau}|S_\tau\rangle\langle S_\tau|$ are introduced between each $\hat{U}_{\Delta\tau}$ so that the partition function $Z = Tre^{-\beta\hat{H}}$ becomes a sum over the classical degrees of freedom associated with the spatial labels of each I_τ and also an additional imaginary time index denoting the location $\tau = 1, 2, \ldots, L_\tau$ of I_τ in the string of operators $\hat{U}_{\Delta\tau}$. The quantity being summed in the calculation of Z is the product of matrix elements $\langle S_\tau|\hat{U}_{\Delta\tau}|S_{\tau+1}\rangle$.

In such WLQMC/GFQMC methods, the SP arises when $\Pi_\tau\langle S_\tau|\hat{U}_{\Delta\tau}|S_{\tau+1}\rangle < 0$. Negative matrix elements are unavoidable for itinerant fermionic models in $D > 1$ because their sign depends on the number of fermions intervening between two particles undergoing exchange, and thus changes as the particle positions are updated. The basis dependence of the SP is apparent by considering intermediate states $|S_\tau\rangle$ chosen to be eigenstates $|\phi_\alpha\rangle$ of $\hat{H}$, with eigenvalues E_α. In that case, the matrix elements are just $e^{-\Delta\tau E_\alpha}$ and thus are trivially positive definite. Of course, because the eigenstates of $\hat{H}$ are unknown, this is not a practical choice in any nontrivial situation. Moreover, the SP can generally be avoided for bosonic or spin models as long as the lattice is bipartite. Nonetheless, even bosonic and spin Hamiltonians can have negative matrix elements on frustrated geometries (*27*), especially for antiferromagnetic models, emphasizing that the SP is not solely a consequence of Fermi statistics.

Auxiliary field QMC (AFQMC) algorithms (*28*–*30*) typically have a much less severe SP than WLQMC (*7*, *31*). They are based on the observation that the trace of an exponential of a quadratic form of fermionic operators can be done analytically, resulting in the determinant of a matrix of dimension set by the cardinality of fermionic operators. The determinant is the product $\Pi_j\left(1 + e^{-\beta\varepsilon_j}\right)$, where ε_j is the noninteracting energy level and is always positive.

If interactions are present, quartic terms in $\hat{H}$ are reduced to quadratic ones with a Hubbard-Stratonovich transformation. The trace of the resulting product of exponentials of quadratic forms can be performed, but now they each depend on a different, i.e., imaginary-time dependent, auxiliary field. The resulting determinant is no longer guaranteed to be positive; the consequence is the SP given that the Hubbard-Stratonovich field

[1]Beijing Computational Science Research Center, Beijing 100193, China. [2]Department of Physics, University of California, Davis, CA 95616, USA.
Correspondence: rmondaini@csrc.ac.cn (R.M.); tarats@csrc.ac.cn (S.T.); scalettar@physics.ucdavis.edu (R.T.S.)

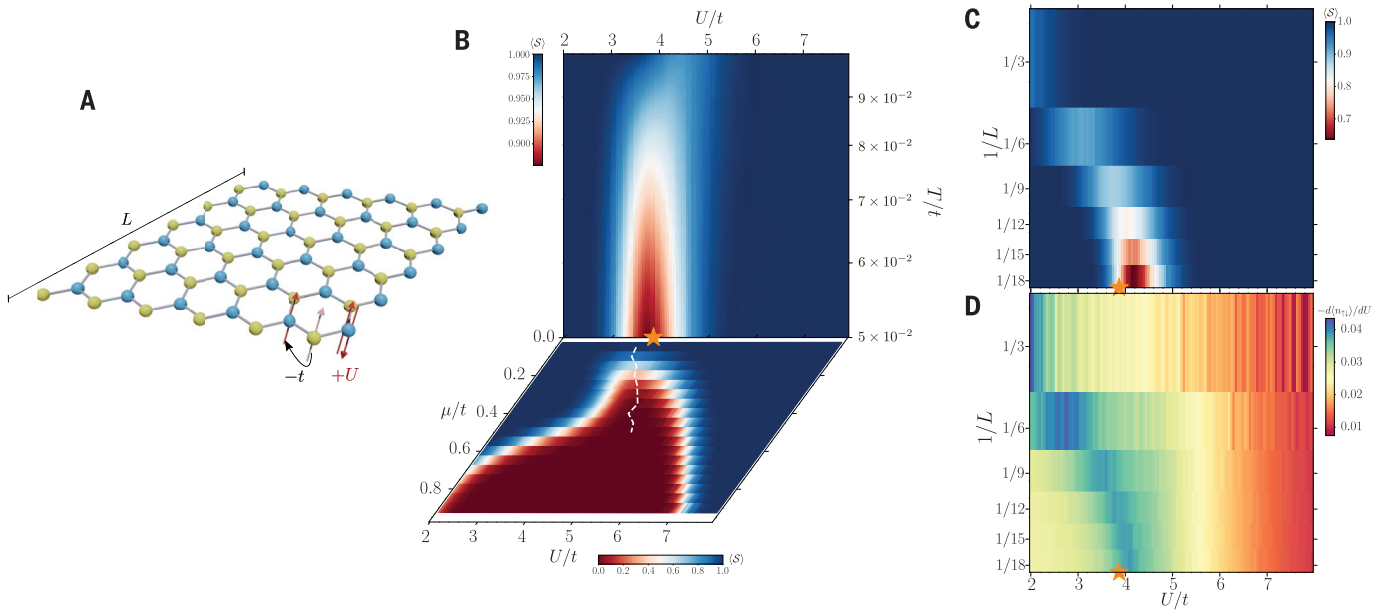

Fig. 1. The SU(2) Hubbard model on the honeycomb lattice. (**A**) Diagram depicting a honeycomb lattice with $N = 2L^2$ sites ($L = 6$ here), accompanied by the relevant terms in $\hat{H}$. (**B**) Contour plot of the average $\langle S \rangle$ in the T/t (μ/t) versus U/t in the upper (lower) panel. Here $L = 9$ and $\mu/t = 0.1$ ($T/t = 1/20$) in the upper (lower) panel. (**C**) Average sign extrapolated with the linear system size L using $T/t = 1/20$ and $\mu/t = 0.1$. (**D**) Similar extrapolation as in (C) but displaying a local quantity (the derivative of the double occupancy), which is an indicator of the QCP. In all panels with data, the prediction for the ground-state phase transition occurring at $U_c/t = 3.869$ (*17*) is depicted by a star marker. In all data, Trotter discretization is chosen as $t\Delta\tau = 0.1$. See fig. S1 for additional observables and fig. S2 for the fermionic flavor-dependent average sign.

needs to be sampled stochastically to compute operator expectation values.

In AFQMC, the trace over fermionic degrees of freedom is done for all species (i.e., all spin and orbital indices α). If there is no hybridization between different α's, each trace gives an individual determinant. In some situations, particle-hole, time-reversal, or other symmetries (*32*–*34*) impose a relation between the determinants for different α's, and as a consequence the negative determinants always come in pairs. Low-temperature (ground-state) properties can be accessed in such "SP-free" cases, and a host of interesting quantum phase transitions has been explored (*35*–*38*).

If such a partnering does not occur, then a reasonable rule of thumb is that the average sign $\langle S \rangle$ is sufficiently bounded away from zero with measurements that exhibit sufficiently small error bars for $T \gtrsim W/20 - W/40$, at intermediate interaction strengths (of the same order as the bandwidth W) (*39*).

The DQMC methodology (*28*, *29*) that we used is a specific implementation of AFQMC. We used the discrete Hubbard-Stratonovich transformation introduced by Hirsch (*40*) and chose the Trotter discretization $\Delta\tau$ such that systematic errors in $\langle S \rangle$ and other observables are of the same order as statistical sampling errors [for additional details, see the materials and methods (*7*)].

We mainly consider models in which two (spin) species of itinerant electrons hop on a lattice with an on-site repulsion, i.e., variants of the Hubbard Hamiltonian,

$$\hat{H} = -\sum_{ij\sigma} t_{ij}\left(\hat{c}^{\dagger}_{i\sigma}\hat{c}_{j\sigma}\right) + \left(\hat{c}^{\dagger}_{j\sigma}\hat{c}_{i\sigma}\right) - \sum_{i\sigma}\mu_i\hat{n}_{i\sigma} + U\sum_i\left(\hat{n}_{i\uparrow} - \frac{1}{2}\right)\left(\hat{n}_{i\downarrow} - \frac{1}{2}\right) \quad (1)$$

Here, $\hat{c}^{\dagger}_{j\sigma}(\hat{c}_{j\sigma})$ are creation (destruction) operators at site i with spin σ and $\hat{n}_{i\sigma} = \hat{c}^{\dagger}_{i\sigma}\hat{c}_{i\sigma}$ is the number operator. In the first model, i and j are near-neighbor (NN) sites on a honeycomb lattice, with $t_{ij} = t$. As a consequence of particle hole symmetry, $\mu_i = 0$ corresponds to half-filling and $\rho = \langle \hat{n}_{i\sigma} \rangle = 1/2$, for arbitrary U and temperature T. For the second model, we consider a $t_{ij} = t$ square lattice with $\mu_i = +\Delta$ on one sublattice and $\mu_i = -\Delta$ on the other, a situation that has an SP even at half-filling, but which is mild enough to allow its phase diagram to be established with reasonable reliability. The third model concerns a single species model with interactions between fermions on neighboring sites, notable because an SP-free QMC formulation exists (*22*, *41*).

All of these models have QCPs that have been located to fairly high precision and so serve as testbeds for demonstrating that the average sign can be used as an alternative means to study the onset of quantum criticality. In our final investigation, we consider the doped, spinful, square lattice Hubbard model, much of the low-temperature physics of which remains shrouded in mystery. We correlate the behavior of the SP with some of the model's properties at intermediate temperature and then describe what might be inferred concerning the presence of a low-temperature superconducting dome.

Semimetal to antiferromagnetic MI on a honeycomb lattice

On a honeycomb lattice (Fig. 1A), the $U = 0$ Hubbard Hamiltonian has a semimetallic density of states that vanishes linearly at $E = 0$. Its dispersion relation $E(k)$ has Dirac points in the vicinity of which the kinetic energy varies linearly with momentum. Unlike the square lattice that displays AF order for all $U \neq 0$, the honeycomb Hubbard model at $T \to 0$ remains a semimetal for small nonzero U, turning to an AF insulator only for U exceeding a critical U_c. Early DQMC and series expansion calculations estimated $U_c \sim 4t$ (*42*), with subsequent studies (*16*, *17*) yielding the more precise value $U_c/t = 3.869$.

The upper panel of Fig. 1B gives $\langle S \rangle$ in the U–T plane. By introducing a small, nonzero $\mu = 0.1$, we can induce a SP that begins to develop at $T/t \sim 0.1$. As T is lowered further, the average sign deviates from $\langle S \rangle = 1$ in a relatively narrow window of U/t close to the known U_c. In turn, we show the $\langle S \rangle$ on the U–μ plane at fixed $T/t = 0.05$ in the lower panel of Fig. 1B. For large μ, the sign is small for a broad swath of interaction values. As μ

decreases, this region pinches down until it terminates close to U_c; the dashed white line displays the minimum $\langle S \rangle$ in the relevant range. In both panels, the behavior of the average sign outlines the quantum critical fan that extends above the QCP.

Figure 1C shows a finite size extrapolation of $\langle S \rangle$ in the $1/L$–U plane, where L is the linear lattice size. Just as $\langle S \rangle$ worsens with increasing β, it is also known to deviate increasingly from $\langle S \rangle = 1$ with growing L (*29*). The extrapolation $L \to \infty$ clearly reveals U_c in the presence of a small chemical potential. So far, we have exclusively used $\langle S \rangle$ in locating U_c. Original investigations used more "traditional" (and more physical) correlation functions such as the AF structure factor and conductivity. For comparison with the evolution of $\langle S \rangle$, Fig. 1D shows one example, the rate of change of the double occupancy $\langle n_{\uparrow\downarrow} \rangle$, again in the $1/L$–U plane. A peak in $-d\langle n_{\uparrow\downarrow} \rangle / dU$ indicates where local moments $\langle m^2 \rangle$ are growing most rapidly. The similarity between Fig. 1, C and D, emphasizes how $\langle S \rangle$ is tracking the physics of the model in a way markedly similar to $\langle m^2 \rangle$. The combination of the three limits, μ, β, and L, unequivocally points out the QCP location; the supplementary materials (*7*) contain further discussion and other observables. Two of these limits can be simultaneously approached by fixing the ratio L_τ / L^z with z, the dynamical critical exponent (*43*).

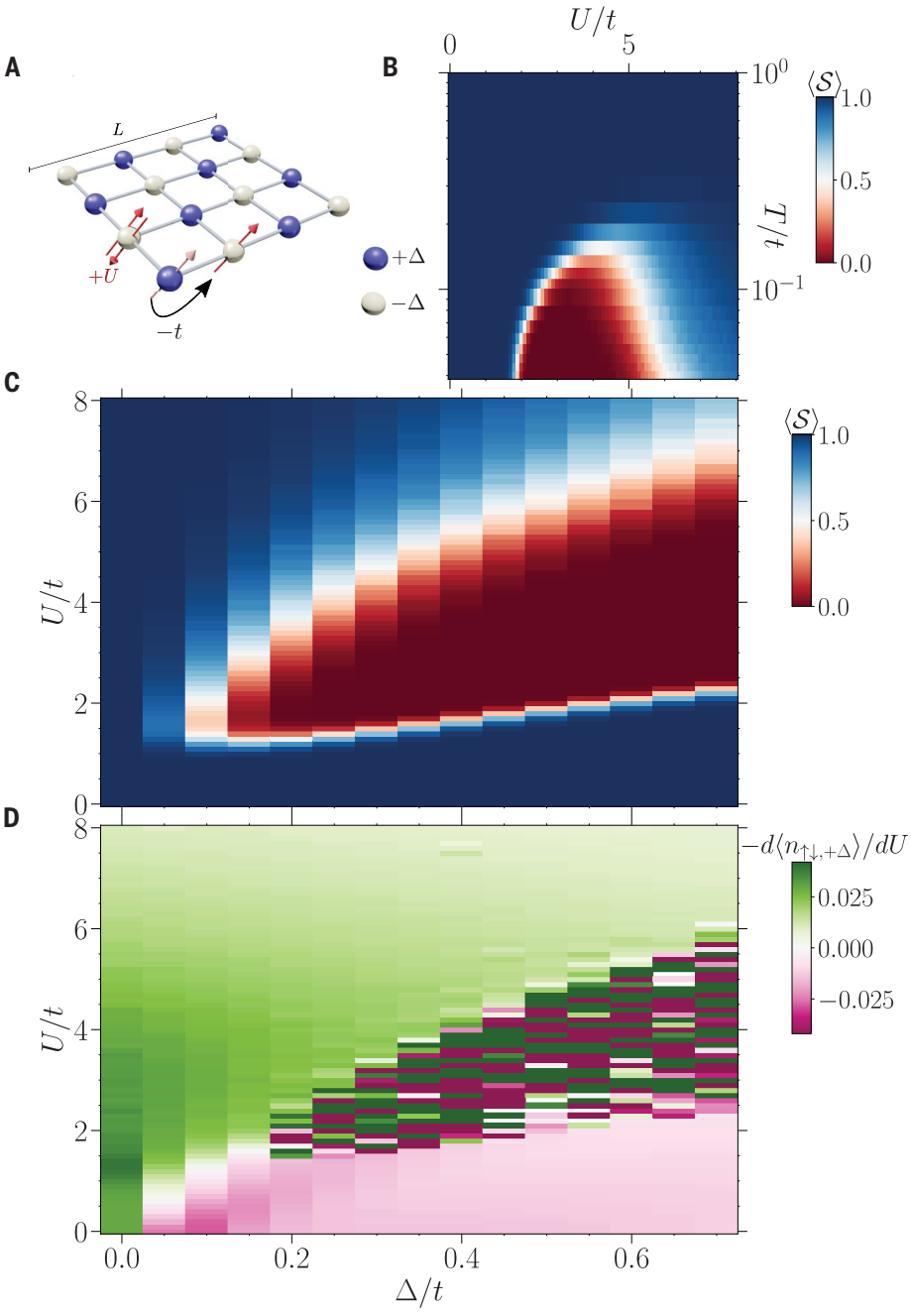

Fig. 2. The SU(2) ionic Hubbard model on the square lattice. (**A**) Diagram depicting a square lattice with $N = L^2$ sites ($L = 4$ here), accompanied by the relevant terms in $\hat{H}$. (**B**) Contour plot of the average $\langle S \rangle$ in the U/t versus T/t plane, with staggered potential $\Delta/t = 0.5$. (**C**) Contour plot of $\langle S \rangle$ as a function of the competing parameters U/t and Δ/t at a temperature $T/t = 1/24$. (**D**) The corresponding derivative of the double occupancy on the $+\Delta$ sites at the same parameters as in (C). In all data, Trotter discretization is chosen as $t\Delta\tau = 0.1$ and the lattice size is $L = 12$. Finite-size analyses are shown in figs. S3 and S4.

Ionic Hubbard BI to AF transition

Among the different types of nonconducting states are BIs, in which the chemical potential lies in a gap in the noninteracting density of states, and MIs, in which strong repulsive interactions prevent hopping at commensurate filling. The evolution from BI to MI is a fascinating issue in condensed-matter physics (*18*–*20*, *44*–*46*). In the ionic Hubbard model that we investigated here, a staggered site energy $\mu_i = \pm\Delta$ on the two sublattices of a square lattice (Fig. 2A) leads to a dispersion relation $E(k) = \pm\sqrt{\varepsilon(k)^2 + \Delta^2}$ with $\varepsilon(k) = -2t\,(\cos k_x + \cos k_y)$. The resulting density of states vanishes in the range $-\Delta < E < +\Delta$ in which the lattice is half-filled, resulting in a BI. The occupation of the "low-energy" sites $\mu_i = -\Delta$ is greater than that of the "high-energy" sites $\mu_i = +\Delta$, so that there is a trivial CDW order associated with an explicit breaking of the sublattice symmetry in the Hamiltonian.

An onsite repulsion U disfavors this density modulation: The potential energy $U\langle n_{\uparrow\downarrow} \rangle$ is higher than that for a uniform occupation. Thus, the driving physics of the BI, the staggered site energy Δ, and that of the MI, the repulsion U, are in competition. Although the simplest scenario is a direct BI to MI transition with increasing U, one of the more exotic possible outcomes is the emergence of a metallic phase when these two energy scales are in balance and neither type of insulator can dominate the behavior. Past DQMC simulations suggest that this less trivial case occurs and have used the temperature dependence of the DC conductivity to bound the metallic phase (*46*, *47*).

Here, we investigated how this physics might be reflected in the average sign. Figure 2B shows $\langle S \rangle$ in the U/t–T/t plane at $\Delta = 0.5t$. As T is lowered, $\langle S \rangle$ deviates from unity for a range of intermediate U values. Figure 2C gives the behavior in the U/t–Δ/t plane at fixed low $T = t/24$. The central result is that $\langle S \rangle$ is small in a region that maps well with the previously determined boundaries of the metallic phase (*46*, *47*). This is emphasized

by comparison with Fig. 2D, which uses one of the "traditional" methods for phase boundary location, namely the behavior of the double occupancy. The BI has a low occupancy and thus very low double occupancy on the +Δ sites. Increasing U smooths out the density so that the double occupancy on the +Δ sites increases: $d\langle\hat{n}_{\uparrow\downarrow,+\Delta}\rangle/dU > 0$. By contrast, in the MI region, $U \gtrsim \Delta$, the physics is that of the usual Hubbard Hamiltonian and double occupancy decreases as U grows: $d\langle\hat{n}_{\uparrow\downarrow,+\Delta}\rangle/dU < 0$.

In the CM region between BI and MI, however, obtaining a relevant signal-to-noise ratio for the traditional observables is exponentially challenging precisely because the average sign vanishes in this region. The "phase diagram" obtained by using $\langle S\rangle$ (Fig. 2C) is very similar to that given by the physical observable, the rate of change of double occupancy with U (Fig. 2D)

As in the determination of the QCP for the spinful Hubbard model on a honeycomb lattice, $\langle S\rangle$ emerges as more than a mere nuisance, but also as a harbinger of the physics. An in-depth similarity between these two situations is discussed in the supplementary materials (*7*), where we show that the BI-metal QCP is again uniquely identified by the $1/L$ scaling of $\langle S\rangle$, in precise analogy with the honeycomb case. These results suggest the existence of a quantum critical region associated with the CM phase and the vanishing $\langle S\rangle$.

An "unnecessary" SP

We now consider spinless fermions, in which the on-site Hubbard interaction U, made irrelevant by the Pauli principle, is replaced by an intersite repulsion V,

$$\hat{H} = -t\sum_{\langle ij\rangle}\left(\hat{c}_i^\dagger\hat{c}_j + \hat{c}_j^\dagger\hat{c}_i\right) + V\sum_{\langle ij\rangle}\hat{n}_i\hat{n}_j \quad (2)$$

Equation 2 provides an example of a model in which the SP can be completely solved by using special techniques such as the fermion bag in the continuous time QMC approach (*35*) or by going to a different basis using a Majorana representation of the fermions in the AFQMC method (*41*), as long as the system is on a bipartite lattice and $V > 0$. The standard Blankenbecler, Scalapino, and Sugar approach (*28*), on the other hand, manifestly displays a SP in the low-temperature regime. Nevertheless, to study the sign and its connection with the underlying physics, we used a Blankenbecler, Scalapino, and Sugar–based algorithm to investigate the system on a honeycomb lattice (Fig. 3A). Consideration of this "unnecessary" SP allows us to address fundamental issues related to the influence of different algorithms on the connection between the SP and the physics of model Hamiltonians.

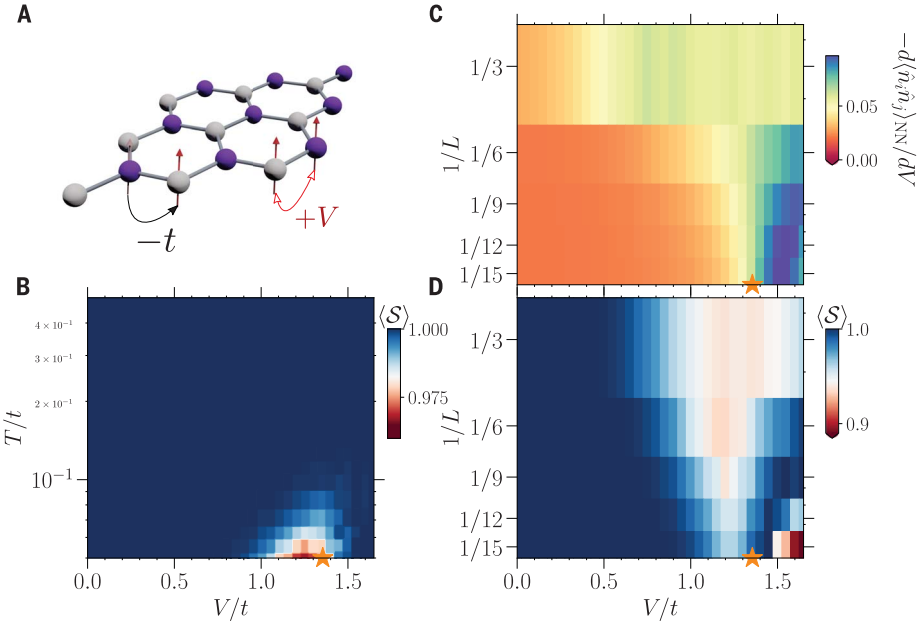

Fig. 3. The U(1) Hubbard model on the honeycomb lattice. (**A**) Schematics of the spinless fermion Hamiltonian (Eq. 2) with NN interaction on a lattice with $L = 3$. (**B**) Temperature extrapolation of the average $\langle S\rangle$ as a function of the NN interaction V/t for a lattice with $L = 9$. (**C**) Extrapolation of the derivative of the NN correlation with respect to V, with the inverse of the linear size L for a range of interactions at a temperature T that scales with the system size $T/t = 0.0375/L\Delta\tau$. (**D**) Same as (C) but showing the average sign. Here, $\langle S\rangle$ marginally increases when tackling larger sizes, indicating that the dynamical critical exponent z in the scaling with L_τ/L^z is > 1 (*7*, *43*); we used $z = 1$ above. In all data, Trotter discretization is chosen as $t\Delta\tau = 0.1$. As for the SU(2) case, the star marker depicts the best known value of the interactions that trigger the Mott insulating phase, here with CDW order at the ground state (*41*). Figure S5 reports a finite-temperature analysis of physical quantities, and fig. S6 analyzes the $\Delta\tau$ influence on $\langle S\rangle$.

At $T = 0$, the model displays a QPT between a Dirac semimetal and an insulating staggered CDW state as the interaction is tuned through a critical value V_c (*22*). At large V, the repulsive interaction favors a CDW state, distinguished from that of the ionic Hubbard model by the fact that there is no staggered external field here; the CDW phase is a result of spontaneous symmetry breaking. As V is reduced, increasing quantum fluctuations caused by hopping finally destroy the CDW state, resulting in a Dirac semimetal for $V < V_c$. Accurate estimates based on SP-free methods yield $V_c \sim 1.35t$ (*41*).

In Fig. 3B, we show a map of the temperature extrapolation of $\langle S\rangle$ as a function of V. The sign shows a clear reduction around the known V_c (denoted by the star). Figure 3D shows the spatial lattice size dependence of the sign, and Fig. 3C, once again, a more "traditional" local variable, the derivative of the nearest-neighbor (NN) density-density correlation $\langle\hat{n}_i\hat{n}_j\rangle_{NN}$ with respect to V. In the CDW phase, increasing V strengthens the staggered order, reducing the NN density correlations, and thus $-d\langle\hat{n}_i\hat{n}_j\rangle_{NN}/dV$ is positive. Conversely, the effect is much smaller in the semimetal state, where the derivative is close to zero. The transition V_c is characterized by a clear downturn in this quantity, which becomes progressively sharper as L increases, as Fig. 3C shows. This variable thus serves as a physical indicator of the QPT, allowing a comparison of Fig. 3, C and D, to demonstrate the connection between the QCP and the behavior of $\langle S\rangle$. In this model, $\langle S\rangle$ is sufficiently well behaved that a study of the finite-temperature CDW transition with DQMC is feasible (*7*) without having to resort to SP-free approaches (*48*).

Square lattice Hubbard model

The essential elements of the physics of the cuprate superconductors include antiferromagnetic order at and near one hole per CuO_2 cell, a superconducting dome upon doping, which typically extends to densities $0.6 \lesssim \rho \lesssim 0.9$, and a "pseudogap"/"strange metal" phase above the dome (*23*, *49*). There are many quantitative, experimentally based phase diagrams of different materials that determine the regions occupied by these phases (*50*). Likewise, there are computational studies of individual (ρ, T, U) points establishing magnetic/charge order (*51*), linear resistivity (*52*), a reduction in the spectral weight for spin excitations (*53*, *54*), and d-wave pairing (*55*, *56*).

Here, we reveal an "SP phase diagram" that bears notable resemblance to the experimental phase diagram. As is well known, the severity of

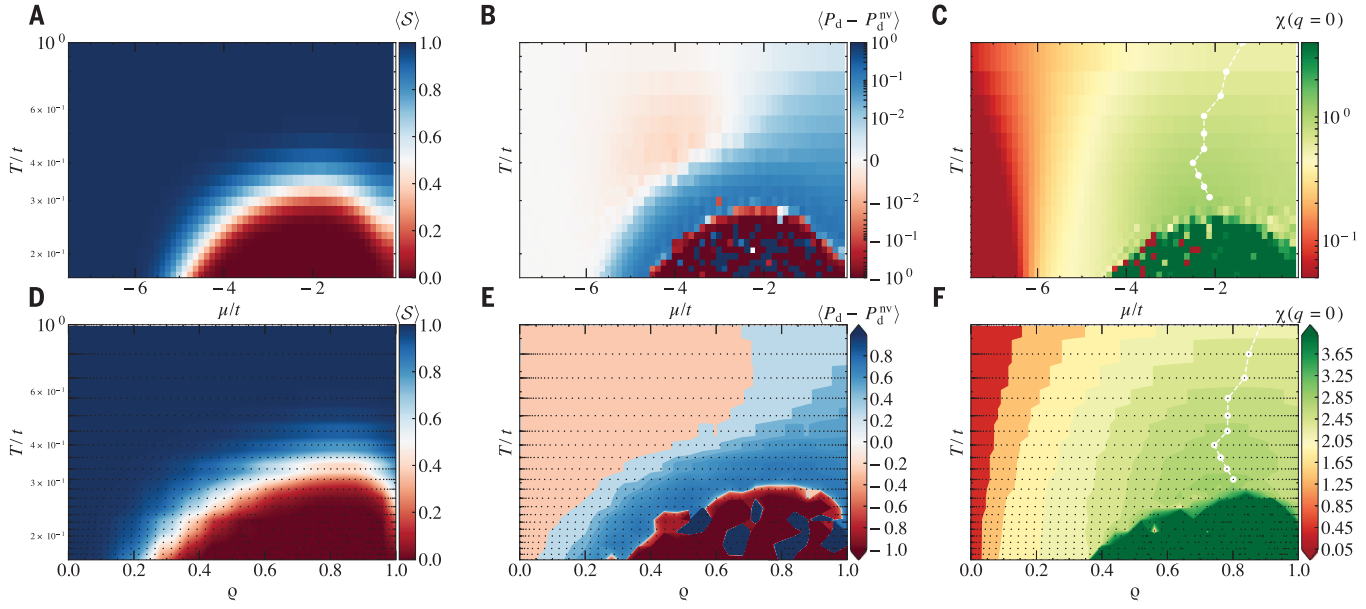

Fig. 4. Square lattice Hubbard model. (**A**) Temperature dependence of the average $\langle S \rangle$ as a function of the chemical potential μ/t for a lattice with $L = 16$, $U/t = 6$, and next-NN hopping $t'/t = -0.2$, values chosen to be close to those in cuprate materials. (**B**) *d*-wave pair susceptibility (with the non-vertex contribution subtracted) for the same parameters. (**C**) Corresponding static spin susceptibility $\chi(q = 0)$. The white markers describe its peak for values at which the average sign is large enough to allow a reliable calculation, which encompasses the pseudogap regime. See the supplementary materials (*7*) for a perspective on the onset of this regime. (**D** to **F**) Corresponding diagrams when converting to the calculated average density. The black markers depict the actual average density extracted from the regular mesh of μ used in the upper panels and where an interpolation of the data is performed. In all data, Trotter discretization is chosen as $t\Delta\tau = 0.0625$. A finite-size analysis (fig. S7), different pairing channels (fig. S8), and the behavior of the spectral weight (figs. S9 and S10) is given in the supplementary materials (*7*). Equivalent results for $t' = 0$ are reported in fig. S11.

the SP itself precludes determination of *d*-wave order in DQMC through "traditional" observables such as the associated correlation functions. However, Fig. 4, which is based on the behavior of the sign itself, is suggestive. We report the average sign (Fig. 4A), the enhancement of the *d*-wave pairing susceptibility over its value in the absence of the pairing vertex (*57*) (Fig. 4B), and the uniform, static spin susceptibility $\chi(q = 0)$ (Fig. 4C) in the T/t–μ/t plane. Figure 4, D to F, shows analogous plots for the T/t–ρ plane (*7*).

The most salient features of this "sign phase diagram" are (i) the "dome" of vanishing $\langle S \rangle$ that occurs in a range of densities $0.4 \lesssim \rho \lesssim 1$ as T is lowered (Fig. 4D), (ii) the enhancement of *d*-wave pairing (Fig. 4E) surrounding the sign dome, and (iii) the magnetic properties being also linked to the $\langle S \rangle$ dome: The trajectory tracing the peak value of $\chi(q = 0)$ as T is decreased terminates precisely at the top of the dome (Fig. 4F). In isolation, the comparisons of the behavior of the sign and the pairing and magnetic responses in the square lattice Hubbard model appear likely to be coincidental. Indeed, the fact that the sign is worse precisely for optimal dopings has been previously discussed, but thought to be just "bad luck" (*32*, *57*–*59*). However, that the known QCPs of the three models discussed in the preceding three sections can be quantitatively linked to the behavior of $\langle S \rangle$ suggests that the sign dome might actually be indicative of the presence of *d*-wave superconductivity.

Discussion and outlook

Early in the history of the study of the SP, a simple connection was noted between the fermionic physics and negative weights in AFQMC: If one artificially constructs two Hubbard-Stratonovich field configurations, one associated with two particle exchanging as they propagate in imaginary time and another with no exchange, one finds that the associated fermion determinants are negative in the former case and positive in the latter. This interesting observation, however, pertains to low density, that is, to the propagation of just two electrons. Another key observation is that the SP can be viewed as being proportional to the exponential of the difference of free energy densities of the original fermionic problem and the one used with the weights in the Monte Carlo sampling taken to be positive, akin to a bosonic formulation of the problem (*13*, *32*). It highlights how intrinsic the SP is in QMC methods. A last important remark is that ordered phases are often associated with a reduction in the importance of configurations that scramble the sign. This is graphically illustrated in the snapshots of (*24*). Although less crisp, similar effects are seen in AFQMC, for example, in considering the evolution from the attractive Hubbard model to the Holstein model with decreasing phonon frequency ω_0. Reducing ω_0 acts to increase the effect of the phonon potential energy term $\hat{P}^2$ in $\hat{H}$, thereby straightening the auxiliary field in imaginary time.

Here, we have shown that the behavior of the average sign $\langle S \rangle$ in DQMC simulations holds information concerning finite density thermodynamic phases and transitions between them: the QCPs in the semimetal to antiferromagnetic MI transition of Dirac fermions, the BI to CM to correlated insulator evolution of the ionic Hubbard Hamiltonian, and the QCP of spinless fermions (even though a sign-problem free formulation exists). Specifically, a rapid evolution of $\langle S \rangle$ marks the positions of QCPs. We have chosen these models as representative examples of QCP physics of itinerant electrons that have been extensively studied in the condensed-matter physics community but speculate that the result is general. In fact, in a model for frustrated spins in a ladder using a completely different QMC method (stochastic series expansion), similar conclusions can be inferred (*60*), further corroborating this generality. Likewise, in the square lattice version of the $U(1)$ Hubbard model that we studied here, with an added

π flux, it can be shown that in the sign-problem free formulation, the QMC weights, when expressed in terms of the square of Pfaffians (Pf), holds similar information, namely that $\langle sgn(Pf)\rangle$ departs from 1 close to the QCP for this model (*61*). These results provide further evidence that the average sign of the QMC weights is inherently connected to the physics of the model in many mutually unrelated models and methods, but an even broader study is necessary to establish this conclusively.

Having established this connection in Hamiltonians with known physics, we have also presented a careful study of the SP for the Hubbard model on a 2D square lattice, which is of central interest to cuprate *d*-wave superconductivity. The intriguing "coincidence" that the SP is the worst at a density $\rho \sim 0.87$, which corresponds to the highest values of the superconducting transition temperature, has been noted previously (*32*, *57*–*59*). It is worth emphasizing that we have not here presented any solution to the SP. However, our work does establish the surprising fact that $\langle S\rangle$ can be used as an "observable" that can quite accurately locate QCPs in models such as the spinful and spinless Hubbard Hamiltonians on a honeycomb lattice and the ionic Hubbard model and also provides a clearer connection between the evolution of the fermion sign and the strange metal/pseudogap and superconducting phases of the iconic square lattice Hubbard model.

REFERENCES AND NOTES

1. B. Hammond, W. Lester, P. Reynolds, *Monte Carlo Methods in Ab Initio Quantum Chemistry, Lecture and Course Notes in Chemistry* (World Scientific, 1994), vol. 1.
2. R. J. Needs, M. D. Towler, N. D. Drummond, P. López Ríos, J. R. Trail, *J. Chem. Phys.* **152**, 154106 (2020).
3. D. Ceperley, *Rev. Mod. Phys.* **67**, 279–355 (1995).
4. W. Foulkes, L. Mitas, R. Needs, G. Rajagopal, *Rev. Mod. Phys.* **73**, 33–83 (2001).
5. J. Carlson *et al*., *Rev. Mod. Phys.* **87**, 1067–1118 (2015).
6. T. Degrand, C. DeTar, *Lattice Methods for Quantum Chromodynamics* (World Scientific, 2006).
7. See the supplementary materials and references therein.
8. T. Esslinger, *Annu. Rev. Condens. Matter Phys.* **1**, 129–152 (2010).
9. I. Bloch, J. Dalibard, S. Nascimbène, *Nat. Phys.* **8**, 267–276 (2012).
10. F. Schäfer, T. Fukuhara, S. Sugawa, Y. Takasu, Y. Takahashi, *Nat. Rev. Phys.* **2**, 411–425 (2020).
11. J. Preskill, *Quantum* **2**, 79 (2018).
12. G. Clemente *et al*., *Phys. Rev. D* **101**, 074510 (2020).
13. M. Troyer, U.-J. Wiese, *Phys. Rev. Lett.* **94**, 170201 (2005).
14. D. Hangleiter, I. Roth, D. Nagaj, J. Eisert, *Sci. Adv.* **6**, eabb8341 (2020).
15. Z.-Q. Wan, S.-X. Zhang, H. Yao, Mitigating sign problem by automatic differentiation. arXiv:2010.01141 [cond-mat.str-el] (2020).
16. Z. Y. Meng, T. C. Lang, S. Wessel, F. F. Assaad, A. Muramatsu, *Nature* **464**, 847–851 (2010).
17. S. Sorella, Y. Otsuka, S. Yunoki, *Sci. Rep.* **2**, 992 (2012).
18. M. Fabrizio, A. O. Gogolin, A. A. Nersesyan, *Phys. Rev. Lett.* **83**, 2014–2017 (1999).
19. L. Craco, P. Lombardo, R. Hayn, G. Japaridze, E. Müller-Hartmann, *Phys. Rev. B* **78**, 075121 (2008).
20. A. Garg, H. R. Krishnamurthy, M. Randeria, *Phys. Rev. Lett.* **112**, 106406 (2014).
21. E. F. Huffman, S. Chandrasekharan, *Phys. Rev. B* **89**, 111101 (2014).
22. L. Wang, P. Corboz, M. Troyer, *New J. Phys.* **16**, 103008 (2014).
23. B. Keimer, S. A. Kivelson, M. R. Norman, S. Uchida, J. Zaanen, *Nature* **518**, 179–186 (2015).
24. J. Hirsch, R. Sugar, D. Scalapino, R. Blankenbecler, *Phys. Rev. B* **26**, 5033–5055 (1982).
25. D. Ceperley, B. Alder, *J. Chem. Phys.* **81**, 5833–5844 (1984).
26. M. A. Lee, K. E. Schmidt, *Comput. Phys.* **6**, 192 (1992).
27. P. Henelius, A. W. Sandvik, *Phys. Rev. B* **62**, 1102–1113 (2000).
28. R. Blankenbecler, D. Scalapino, R. Sugar, *Phys. Rev. D Part. Fields* **24**, 2278–2286 (1981).
29. S. R. White *et al*., *Phys. Rev. B* **40**, 506–516 (1989).
30. S. Zhang, J. Carlson, J. E. Gubernatis, *Phys. Rev. B* **55**, 7464–7477 (1997).
31. M. Iazzi, A. A. Soluyanov, M. Troyer, *Phys. Rev. B* **93**, 115102 (2016).
32. E. Y. Loh Jr. *et al*., *Phys. Rev. B* **41**, 9301–9307 (1990).
33. C. Wu, S.-C. Zhang, *Phys. Rev. B* **71**, 155115 (2005).
34. Z.-X. Li, Y.-F. Jiang, H. Yao, *Phys. Rev. Lett.* **117**, 267002 (2016).
35. S. Chandrasekharan, *Phys. Rev. D Part. Fields Gravit. Cosmol.* **82**, 025007 (2010).
36. E. Berg, M. A. Metlitski, S. Sachdev, *Science* **338**, 1606–1609 (2012).
37. L. Wang, Y.-H. Liu, M. Iazzi, M. Troyer, G. Harcos, *Phys. Rev. Lett.* **115**, 250601 (2015).
38. Z.-X. Li, H. Yao, *Annu. Rev. Condens. Matter Phys.* **10**, 337–356 (2019).
39. This is just a rough guideline; the precise onset of the SP is determined by lattice geometry, doping (chemical potential), and interaction strength. A catalog of the SP in DQMC for the single-band Hubbard model in different situations is given in (*59*).
40. J. Hirsch, *Phys. Rev. B* **28**, 4059–4061 (1983).
41. Z.-X. Li, Y.-F. Jiang, H. Yao, *Phys. Rev. B* **91**, 241117 (2015).
42. T. Paiva, R. Scalettar, W. Zheng, R. Singh, J. Oitmaa, *Phys. Rev. B* **72**, 085123 (2005).
43. H. Rieger, A. P. Young, *Phys. Rev. Lett.* **72**, 4141–4144 (1994).
44. A. Kampf, M. Sekania, G. Japaridze, P. Brune, *J. Phys. Condens. Matter* **15**, 5895–5907 (2003).
45. A. Garg, H. R. Krishnamurthy, M. Randeria, *Phys. Rev. Lett.* **97**, 046403 (2006).
46. N. Paris, K. Bouadim, F. Hebert, G. G. Batrouni, R. T. Scalettar, *Phys. Rev. Lett.* **98**, 046403 (2007).
47. A. Chattopadhyay, S. Bag, H. R. Krishnamurthy, A. Garg, *Phys. Rev. B* **99**, 155127 (2019).
48. S. Hesselmann, S. Wessel, *Phys. Rev. B* **93**, 155157 (2016).
49. A. Damascelli, Z. Hussain, Z.-X. Shen, *Rev. Mod. Phys.* **75**, 473–541 (2003).
50. P. A. Lee, N. Nagaosa, X.-G. Wen, *Rev. Mod. Phys.* **78**, 17–85 (2006).
51. H.-C. Jiang, T. P. Devereaux, *Science* **365**, 1424–1428 (2019).
52. E. W. Huang, R. Sheppard, B. Moritz, T. P. Devereaux, *Science* **366**, 987–990 (2019).
53. M. Randeria, N. Trivedi, A. Moreo, R. T. Scalettar, *Phys. Rev. Lett.* **69**, 2001–2004 (1992).
54. A.-M. S. Tremblay, B. Kyung, D. Sénéchal, *Low Temp. Phys.* **32**, 424–451 (2006).
55. T. A. Maier, M. Jarrell, T. C. Schulthess, P. R. C. Kent, J. B. White, *Phys. Rev. Lett.* **95**, 237001 (2005).
56. T. A. Maier *et al*., *Nat. Commun.* **7**, 11875 (2016).
57. S. R. White, D. J. Scalapino, R. L. Sugar, N. E. Bickers, R. T. Scalettar, *Phys. Rev. B* **39**, 839–842 (1989).
58. D. Scalapino, "Does the Hubbard model have the right stuff?," in *Proceedings of the International School of Physics*, R. A. Broglia, J. R. Schrieffer, eds. (North-Holland, 1994); pp. 95–122.
59. V. Iglovikov, E. Khatami, R. Scalettar, *Phys. Rev. B* **92**, 045110 (2015).
60. S. Wessel, B. Normand, F. Mila, A. Honecker, *SciPost Phys.* **3**, 005 (2017).
61. A. Goetz, S. Beyl, M. Hohenadler, F. F. Assaad, Langevin dynamics simulations of the two-dimensional Su-Schrieffer-Heeger model. arXiv:2102.08899 [cond-mat.str-el] (2021).
62. R. Mondaini, S. Tarat, R. T. Scalettar, Data for: Quantum critical points and the sign problem, Zenodo (2021); https://doi.org/10.5281/zenodo.5575501.
63. "QUEST: QUantum Electron Simulation Toolbox" (UC Davis, 2009); https://www.cs.ucdavis.edu/~bai/QUEST_public/.

ACKNOWLEDGMENTS

We acknowledge insightful discussions with S.-J. Hu and H.-Q. Lin. **Funding:** R.T.S. was supported by grant DE-SC0014671 funded by the US Department of Energy, Office of Science. R.M. acknowledges support from the National Natural Science Foundation of China (NSFC grants NSAF-U1930402, 11974039, 12050410263, and 12111530010). Computations were performed on the Tianhe-2JK at the Beijing Computational Science Research Center. **Author contributions:** R.T.S proposed the original idea for the honeycomb lattice; R.M. suggested its extension to the ionic and spinless fermion cases. All authors considered the square lattice Hubbard model, performed numerical simulations, analyzed data, and cowrote the manuscript. **Competing interests:** The authors declare no competing interests. **Data and materials availability:** All data needed to reproduce the conclusions in this study are present in the main text or the supplementary materials. Data presented in the figures are deposited at Zenodo (*62*), and input files for QUEST codes, which can be used to reproduce the results, are available at (*63*).

SUPPLEMENTARY MATERIALS

science.org/doi/10.1126/science.abg9299
Supplementary Text
Figs. S1 to S11
References (*64*–*167*)

4 February 2021; accepted 15 December 2021
10.1126/science.abg9299

Quantum critical points and the sign problem

R. MondainiS. TaratR. T. Scalettar

Science, 375 (6579), • DOI: 10.1126/science.abg9299

Unexpected benefits of the sign problem

Solving challenging problems in quantum many-body physics often involves using numerical Monte Carlo methods. However, in the most interesting regime of strong interactions and low temperatures, the so-called sign problem can make calculations intractable. Mondaini *et al*. studied the severity of the sign problem quantitatively in several representative models. The researchers found that quantum critical behavior in these models correlated with the regions in the phase diagram where the sign problem was most pronounced. Viewed as a diagnostic for quantum criticality, the sign problem then becomes a tool (in addition to being a nuisance). —JS

Science (ISSN) is published by the American Association for the Advancement of Science. 1200 New York Avenue NW, Washington, DC 20005. The title *Science* is a registered trademark of AAAS.